On the symmetry of cylindrical implosions driven by a rotating beam of fast ions

M. M. Basko[a)]
Gesellschaft für Schwerionenforschung, Planckstrasse 1, D-64291 Darmstadt, Germany

T. Schlegel
TU Darmstadt, Institut für Kernphysik, Schloßgartenstrasse 9, D-64289 Darmstadt, Germany

J. Maruhn
Institut für Theoretische Physik, Universität Frankfurt, D-60054 Frankfurt, Germany

(Received 7 March 2003; accepted 23 December 2003; published online 1 April 2004)

Cylindrical implosions driven by intense beams of heavy ions are one of the promising ways to create high energy density states in matter. To ensure the needed azimuthal symmetry of the beam energy deposition, it was proposed [Sharkov *et al.*, Nucl. Instrum. Methods Phys. Res. A **464**, 1 (2001)] to rotate the ion beam around the target axis. Combining analytical calculations with two-dimensional hydrodynamic simulations, a lower limit is established on the frequency ν of the beam rotation dictated by the target hydrodynamics. This limit is shown to be directly proportional to the desired radial convergence ratio C_r for stepwise beam power profiles, and to $C_r^{1/2}$ for smooth pulses. With a smooth pulse, 6–10 beam revolutions per pulse should be sufficient to reach $C_r \simeq 30$, while a stepwise pulse requires $\simeq 100$ revolutions. Also, the upper bound on the asymmetry of the elliptical focal spot of a rotating ion beam is calculated. © *2004 American Institute of Physics.* [DOI: 10.1063/1.1650352]

I. INTRODUCTION

With the advent of intense beams of fast heavy ions,[1–4] an attractive possibility arises to conduct cylindrical implosion experiments with a high degree of radial convergence.[5] In particular, such implosions would open a way to creating matter states at energy density levels unattainable by other laboratory methods.[5,6] Also, highly symmetric cylindrical implosions driven directly by heavy ion beams are crucial for certain schemes of the inertial confinement fusion.[7,8]

Cylindrical implosions with high radial convergence require high degree of azimuthal uniformity of the beam irradiation, especially when a cold pusher is used to compress the sample material in the central cavity.[5] To ensure the required symmetry of beam irradiation, it was proposed in Ref. 3 to rotate the ion beam around the cylindrical target axis by means of a corresponding beam wobbler. Presently, first efforts have been undertaken at the Institute for Theoretical and Experimental Physics (ITEP, Moscow, Russia), and at the Gesellschaft für Schwerionenforschung (GSI, Darmstadt, Germany) to construct and test such a wobbler. One of the key parameters that has to be determined before laying out the wobbler design is the frequency of the beam rotation ν [Hz, or revolutions per second]. The principal goal of this work has been to analyze the constraints on the wobbler frequency ν, and on the asymmetry of the beam focal spot dictated by the physics of target implosion.

In Sec. II we describe the statement of the problem and introduce the target structure and the basic notation. We solve our problem by combining analytical calculations (Sec. III) with two-dimensional (2D) hydrodynamical simulations (Sec. IV). The analytical estimates are based on simplifying assumptions that may be not quite adequate for realistic experimental conditions, and, for this reason, should only be considered as a useful auxiliary in the interpretation of the results of 2D simulations. Although our main results are expressed in a dimensionless form and can be applied over a wide range of the beam and target parameters, the 2D numerical simulations have been centered around a base set of parameters [see Eq. (31) below] that are considered to be realistic for the near-future TWAC[1] and SIS-200[4] facilities at, respectively, ITEP (Moscow) and GSI (Darmstadt). Since only the ratio $E_b/\mathcal{R}$ of the total beam energy E_b to the effective range $\mathcal{R}$ [defined in Eq. (13) below] is relevant for the problem addressed here, our base parameters correspond roughly to 1.2×10^{13} ions of Co with the kinetic energy of 0.7 GeV/u ($E_b=80$ kJ, $\mathcal{R}\approx40$ g/cm^2),[1] or to 10^{12} ions of U with the kinetic energy of 0.5 GeV/u ($E_b=20$ kJ, $\mathcal{R}\approx10$ g/cm^2).[4] We find that, for any smooth beam power profile, already 6–10 beam revolutions over the pulse duration ensure adequate azimuthal symmetry of cylindrical implosions allowing to reach convergence ratios $C_r \gtrsim 30$.

After all the principal results of this work had been obtained, our attention was drawn to a new publication[9] devoted to the same problem. The authors of this paper made a simple analytical estimate of the pressure nonuniformities due to a finite frequency ν of the beam rotation for the case of the box pulse profile. As it is clear from the results of our work, such an estimate is not sufficient for establishing a reliable lower limit on ν dictated by the desired symmetry of

[a)]On leave from Institute for Theoretical and Experimental Physics, Moscow, Russian Federation. Electronic mail: basko@vitep1.itep.ru

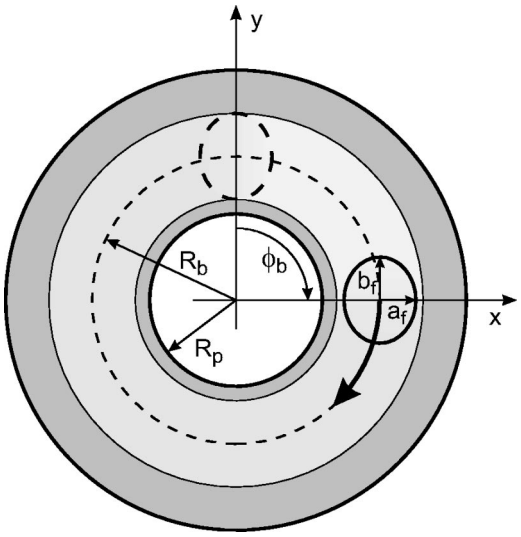

FIG. 1. Target configuration for cylindrical implosions driven by a rotating ion beam.

the imploded state, even for the simplest case of the box pulse.

II. PROBLEM SETUP AND NOTATION

Consider a tube-like cylindrical target consisting of a solid (typically of heavy metal) liner shell which encloses a central cavity filled with a low density gas (see Fig. 1). The initially uniform liner is subdivided into three adjacent layers: the payload (initially at $R_p<r<R_{a1}$), the absorber (initially at $R_{a1}<r<R_{a2}$), and the tamper (initially at $R_{a2}<r<R$). A beam of fast ions, propagating along the axial direction, rotates around the cylinder axis with a cyclic frequency

$$\nu=\frac{1}{2\pi}\frac{d\phi_b}{dt} \tag{1}$$

and deposits its energy inside the absorber annulus $R_{a1}=R_b-r_f<r<R_{a2}=R_b+r_f$; here R_b is a fixed radius of the circular beam orbit, ϕ_b is the azimuth of the center of the beam focal spot measured clockwise from the ''north pole''—as is shown in Fig. 1. In a general case, we assume that the focal spot of the rotating beam is an ellipse with semiaxes a_f and b_f; then $r_f=\max\{a_f,b_f\}$.

In this work we investigate departures from the ideal cylindrical symmetry of implosion in the (r,ϕ) plane which arise from the following two types of azimuthal nonuniformities in the beam energy deposition:

(i) cyclic nonuniformities that are caused by the finite and/or noninteger number of beam revolutions; these nonuniformities come to a foreground when the beam focus is nearly an ideal circle; they set a lower limit on the beam rotation frequency ν;

(ii) focal nonuniformities caused by a parallel displacement of a noncircular focal spot along the beam orbit; these nonuniformities will be present even for an infinitely large value of ν; they set an upper limit on the allowed asymmetry of the rotating focal spot.

We ignore any possible distortion and misalignment of the beam orbit, and assume a perfect uniformity along the cylinder length (z axis).

The main focus of this work is on the cyclic nonuniformities. When investigating this type of perturbations, we assume that the focal spot is a circle with radius r_f. The role of the focal nonuniformities is evaluated only for the simplest noncircular shape, i.e., for an elliptical focal spot with semiaxes a_f and b_f along, respectively, the global x and y axis in the (r,ϕ) plane (see Fig. 1). As a result, we obtain an upper limit for the dimensionless asymmetry parameter $|\delta_f|$, where δ_f is defined as

$$\delta_f=\frac{a_f-b_f}{\sqrt{a_f b_f}}. \tag{2}$$

To all practical purposes, our problem can be adequately addressed in the framework of pure 2D hydrodynamics, with no regard for such dissipation mechanisms as heat conduction, viscosity, radiative transport, etc. As in many such problems, the results can be expressed in terms of dimensionless parameters. An obvious choice for the dimensionless beam rotation frequency is the total number of beam revolutions,

$$\overline{\nu}=\nu t_b, \tag{3}$$

over the ion pulse duration t_b.

In general, the lower limit on $\overline{\nu}$ (or the upper limit on $|\delta_f|$) will be determined by several dimensionless parameters which characterize the problem. By far the most important of them is the radial convergence ratio C_r that is to be achieved in the course of implosion. We define the radial convergence with respect to the interface between the payload and the central gaseous cavity, whose initial position is at $r=R_p$. For noncircular shapes of this interface at later times, we use the total area S_g inside the gaseous cavity to calculate C_r as

$$C_r=\frac{R_p}{(S_g/\pi)^{1/2}}. \tag{4}$$

Clearly, higher values of C_r will require higher values of $\overline{\nu}$ and lower values of $|\delta_f|$.

Other relevant dimensionless parameters in our problem are (i) the ratio t_b/t_{im} of the pulse duration t_b to the implosion time t_{im}, (ii) the ratio r_f/R_b of the beam focal radius r_f to the beam orbit radius R_b, (iii) the relative (with respect to the half of the absorber mass) mass of the payload μ_{pa}, and, possibly, some other—depending on the complexity of the target design and thermodynamic properties of the materials used. In particular, the value of t_b/t_{im} (which for hydrodynamically consistent target configurations must be below 1) controls the interplay of two different effects relevant for both the cyclic and the focal nonuniformities: the effect of nonuniform (over the azimuthal angle ϕ) total energy deposition, and the effect of systematic retardation in the energy deposition at larger ϕ due to the finite angular velocity of the beam rotation. The effect of retardation dominates, for example, when a box pulse with an integer number of beam revolutions is used: the total energy deposition is perfectly uniform (for a circular focal spot) whereas the absorber segment at, say, $\phi=3\pi/2$ is heated systematically half a period

later than the segment at $\phi=\pi/2$. Clearly, the effect of azimuthal retardation vanishes in the limit of $t_b/t_{im}\ll 1$, whereas the nonuniformity of the energy deposition does not.

Finally, the solution to our problem turns out to be sensitive to the temporal power profile of the ion beam $W_b(t)$. To characterize the temporal pulse shape, we introduce a dimensionless pulse profile

$$\Omega(\tau)=t_b\frac{W_b(\tau t_b)}{E_b},\quad 0\leqslant\tau\equiv\frac{t}{t_b}\leqslant 1, \tag{5}$$

normalized by the condition

$$\int_0^1\Omega(\tau)d\tau=1, \tag{6}$$

here

$$E_b=\int_0^{t_b}W_b(t)dt \tag{7}$$

is the total beam energy. As specific examples, we consider the following pulse shapes:

$$\Omega(\tau)=\begin{cases}1, & \text{box pulse,}\\ 2(1-|2\tau-1|), & \text{triangular pulse,}\\ 6\tau(1-\tau), & \text{parabolic pulse,}\\ 2\sin^2(\pi\tau), & \text{sine-squared pulse.}\end{cases} \tag{8}$$

III. ANALYTICAL EVALUATION

Analytical calculations can only be done under certain simplifying assumptions that may be not quite realistic for experimental conditions. Hence, the analytical results obtained below should be considered as only providing useful guidelines and scaling relationships which, in their turn, should be verified and rectified in 2D numerical simulations.

Our main simplifying assumption is that the geometrical thicknesses of both the absorber and the payload layers are small compared to their radii. Then, the radial motion of each ϕ element of a thin payload can be treated as locally planar and independent of the conditions at other ϕ values. Clearly, only long-wavelength (with respect to the payload thickness) perturbations can be treated under such an approximation.

To relate the radial displacement of the imploding payload to the local (at a given ϕ) energy deposition, we have to apply a certain model for the payload acceleration. Here one has to distinguish between two qualitatively different regimes: a slow (quasiadiabatic) acceleration by a relatively long ion pulse, and a fast (shock-like) acceleration by the first shock launched from the absorber into the payload after a short ion pulse. The separation between the two regimes is controlled by the parameter t_b/t_{hp}, where t_{hp} is the time of sound propagation across the payload; for the cases of interest here we typically have $t_{hp}\simeq 10-20$ ns. Having in mind ion pulses with $t_b\simeq 50-200$ ns, we apply a simple analytical model for the *quasiadiabatic* payload acceleration based on a self-similar solution for a planar layer driven by a specified volumetric heating (see Appendix A).

The relation between the radial convergence ratio C_r and the initial nonuniformity of the implosion is established by setting a limit on the maximum allowed perturbation of the gas-payload interface $r_p=r_p(t,\phi)$ at the end of implosion t: we assume that the ratio between the maximum (over azimuth ϕ) and the minimum values of $r_p(t,\phi)$ should not exceed $\max_\phi\{r_p(t,\phi)\}:\min_\phi\{r_p(t,\phi)\}=2:1$. For an elliptical distortion this results in the condition

$$\frac{|\delta r_p|}{R_p}=\frac{\max_\phi\{r_p(t,\phi)\}-\min_\phi\{r_p(t,\phi)\}}{R_p}\leqslant\frac{1}{\sqrt{2}\,C_r}, \tag{9}$$

where $R_p=r_p(0,\phi)$ is the initial radius of the gas-payload interface, and C_r is the convergence ratio at time t evaluated according to Eq. (4). Of practical interest are, of course, the values $C_r\gg 1$.

Thus, to obtain a corresponding limit on $\overline{\nu}$ (or on $|\delta_f|$), we have, in the first place, to relate the perturbation $|\delta r_p|/R_p$ to the azimuthal nonuniformity of the energy deposition $|\delta\epsilon_{\rm tot}|/\epsilon_{\rm tot}$, and then to calculate $|\delta\epsilon_{\rm tot}|/\epsilon_{\rm tot}$ as a function of $\overline{\nu}$ (or of $|\delta_f|$) and apply the criterion (9).

A. Cyclic nonuniformities

Cyclic nonuniformities are due to a finite number $\overline{\nu}$ of the beam revolutions. Here we assume a perfectly circular focal spot with radius r_f. The analysis becomes particularly simple in the limit of $t_b\ll t_{im}$, when we can neglect the effect of retardation. For a quasiadiabatic payload acceleration, and at $C_r\gg 1$ we have

$$\frac{|\delta r_p|}{R_p}=\frac{1}{2}\frac{|\delta\epsilon_{\rm tot}|}{\epsilon_{\rm tot}}, \tag{10}$$

where $\epsilon_{\rm tot}=\epsilon_{\rm tot}(\phi)$ is the mean (over the radial thickness of the absorber) total specific energy deposition at azimuth ϕ. Equation (10) follows from a simple general consideration that both the implosion velocity and the distance travelled by the payload by time $t=t_{im}\gg t_b$ are directly proportional to $\epsilon_{\rm tot}^{1/2}$, while the dependence on other parameters can be ignored so long as they experience no ϕ variation. This result can, of course, be obtained directly from Eq. (A11) of the self-similar solution, in which $Y(t)-Y_0$ should be identified with $R_p-r_p(t,\phi)$. Note that in the limit of a shock-like acceleration of the payload Eq. (10) may become inapplicable: for not too strong shocks breaking out of a solid the resulting velocity is directly proportional to the pressure in the absorber,[10] which, for short pulses with $t_b\ll t_{hp}$ and a massive absorber, is directly proportional to $\epsilon_{\rm tot}$.

For a thin absorber, the mean specific energy deposited by time t at a given azimuth ϕ can be written as

$$\epsilon(t,\phi)=\sum_k\Delta\epsilon_k(\phi),\quad 0<t_k<t, \tag{11}$$

where

$$\Delta\epsilon_k(\phi)=\frac{W_b(t_k)}{\nu S_a\mathcal{R}},\quad t_k=\nu^{-1}\left(\frac{\phi}{2\pi}+k-1\right). \tag{12}$$

In other words, each time the rotating beam sweeps across the selected absorber element, the specific deposited energy $\epsilon(t,\phi)$ increases in a jump [more precisely, on a time scale of $r_f/(2\pi R_b\nu)\ll\nu^{-1}$] by an amount $\Delta\epsilon_k(\phi)$ (see Fig. 2). Here $k=1,2,3,\ldots$ is the sequential revolution number,

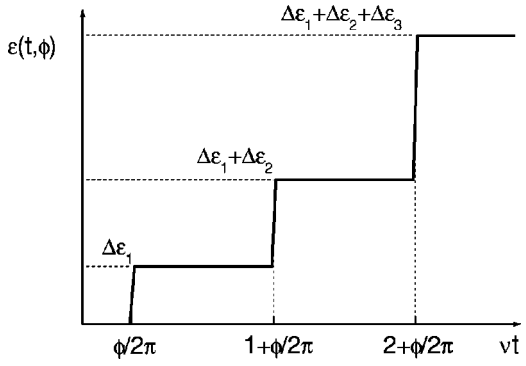

FIG. 2. Time dependence of the mean (averaged over the absorber thickness) specific energy deposition by a rotating ion beam in a target with a thin absorber at a given azimuth ϕ.

$S_a = 4\pi r_f R_b$ is the total absorber area sweeped by the rotating beam, and $\mathcal{R}$ is the effective ion range in the absorber material defined by

$$\frac{1}{\mathcal{R}} = \frac{1}{E_i}\left|\frac{dE_i}{\rho_a\, dz}\right|, \tag{13}$$

where E_i is the energy of individual beam ions, ρ_a is the absorber density. Note that the dependence of $\Delta\epsilon_k$ on ϕ occurs only through the argument t_k of the temporal profile of the beam power $W_b(t)$.

To calculate the total energy deposition $\epsilon_{\mathrm{tot}}(\phi)$ for times $t > t_b$, we have to perform summation in Eq. (11) over the entire beam pulse. The result is obtained straightforwardly for the two simplest cases, namely, for the box pulse,

$$\frac{|\delta\epsilon_{\mathrm{tot}}|}{\epsilon_{\mathrm{tot}}} = \frac{\max\{\epsilon_{\mathrm{tot}}(\phi)\} - \min\{\epsilon_{\mathrm{tot}}(\phi)\}}{E_b/(S_a\mathcal{R})} = \frac{1}{\bar{\nu}} \times \begin{cases} 0, & \Delta\bar{\nu} = 0, \\ 1, & \Delta\bar{\nu} \neq 0, \end{cases} \tag{14}$$

and for the triangular pulse,

$$\frac{|\delta\epsilon_{\mathrm{tot}}|}{\epsilon_{\mathrm{tot}}} = \frac{2}{\bar{\nu}^2} \times \begin{cases} \Delta\bar{\nu}, & \text{even } [\bar{\nu}], \\ (1-\Delta\bar{\nu}), & \text{odd } [\bar{\nu}], \end{cases} \tag{15}$$

(for details see Appendix B). Here $[\bar{\nu}]$ denotes the integer part of $\bar{\nu}$, $0 \leqslant \Delta\bar{\nu} = \bar{\nu} - [\bar{\nu}] \leqslant 1$ is the fractional part of $\bar{\nu}$, and $E_b/(S_a\mathcal{R})$ is the mean (over the entire absorber area S_a) total specific energy deposition in the absorber.

Equations (14) and (15) reveal an important general difference between stepwise and smooth pulse shapes: for stepwise pulses the azimuthal nonuniformity of the beam energy deposition decreases as $\bar{\nu}^{-1}$ with the increasing number of beam revolutions $\bar{\nu}$, whereas for smooth pulses it decreases much faster, as $\bar{\nu}^{-2}$. The distinction between the smooth and the stepwise pulses lies in that the beam power $W_b(t)$ of a smooth pulse is a continuous function of t, which increases from zero to its peak value and drops back to zero smoothly, i.e., on the time scale t_b of the total pulse duration. In contrast, the power $W_b(t)$ of a stepwise pulse experiences one or more jumps (on a time scale shorter than ν^{-1}) by a significant amount compared to its peak value.

For a broad class of smooth pulses with a continuous first derivative $\Omega'(\tau) \equiv d\Omega/d\tau$ inside the interval $0 < \tau < 1$, one can derive a general expression for the first term $O(\bar{\nu}^{-2})$ in the series expansion of $\delta\epsilon_{\mathrm{tot}}/\epsilon_{\mathrm{tot}}$ in powers of $\bar{\nu}^{-1}$ (see Appendix B). In particular, for a symmetric pulse with $\Omega'(1) = -\Omega'(0)$, we have

$$\frac{|\delta\epsilon_{\mathrm{tot}}|}{\epsilon_{\mathrm{tot}}} = \frac{\Omega'(0)}{4\bar{\nu}^2} \times \left\{ \begin{array}{ll} (1-\Delta\bar{\nu})^2, & 0 \leqslant \Delta\bar{\nu} \leqslant \frac{1}{2}, \\ \Delta\bar{\nu}^2, & \frac{1}{2} \leqslant \Delta\bar{\nu} \leqslant 1, \end{array} \right\} + O(\bar{\nu}^{-3}). \tag{16}$$

When we use Eq. (16) to compare the parabolic, $\Omega = 6\tau(1-\tau)$, or, say, the sine-like, $\Omega = 0.5\pi \sin(\pi\tau)$, pulses with the triangular one, we find that the maximum variation $|\delta\epsilon_{\mathrm{tot}}|/\epsilon_{\mathrm{tot}} = 2/\bar{\nu}^2$ occurs in a triangular pulse with an odd number of revolutions $\bar{\nu}$. Using this "worst" value for smooth pulses, and the box-pulse result (14) as the worst value for stepwise pulses, we obtain from Eqs. (9) and (10) the following analytical constraints on the total number of beam revolutions:

$$\bar{\nu} \gtrsim \begin{cases} 2^{-1/2} C_r, & \text{stepwise pulse}, \\ 2^{1/4} C_r^{1/2}, & \text{smooth pulse}. \end{cases} \tag{17}$$

Note that, as discussed in Sec. IV A, the pulses with higher orders of smoothness [i.e., with $\Omega'(0) = \Omega'(1) = 0,...$] appear to be of no practical interest.

The expressions above have been obtained with no regard for the effect of retardation, i.e., in the limit of $t_b \ll t_{im}$. Here we argue that in general the effect of retardation can alter the proportionality factors in Eq. (17) but not the exponents in the power dependence on C_r. For stepwise pulses this is rather obvious, simply because the maximum time of delay in the energy deposition at different ϕ is ν^{-1}, and the maximum relative difference of the payload displacement at different ϕ cannot be larger than of the order of $\bar{\nu}^{-1}$. For smooth pulses the argument is somewhat more involved.

As it is illustrated by the self-similar solution in Appendix A [namely, by Eq. (A11), in which $Y(t) - Y_0$ should be identified with $R_p - r_p(t,\phi)$], the radial displacement of the payload at a given ϕ is governed by the temporal history of $\epsilon(t,\phi)$, which, in addition, depends on ν as a parameter. The expression (11) for $\epsilon(t,\phi,\nu)$ is nothing else but a finite-difference trapezoidal-rule approximation to the integral $(S_a\mathcal{R})^{-1}\int_0^t W_b(t')\,dt'$ on a discrete mesh with $[t\nu]$ cells over the time interval $(0,t)$. As is well known, the finite-difference error of such an approximation for any continuous function $W_b(t)$ is of the order of $(t\nu)^{-2}$. In other words, the general form of the series expansion of $\epsilon(t,\phi,\nu)$ in powers of $\bar{\nu}^{-1}$ will be

$$\epsilon(t,\phi,\nu) = \frac{1}{S_a\mathcal{R}}\int_0^t W_b(t')dt' + \frac{\epsilon_2(t,\phi)}{\nu^2} + O(\nu^{-3}). \tag{18}$$

Since the first (main) term on the right-hand side of Eq. (18) does not depend on ϕ, and since the implosion time $t_{im} \gtrsim t_b$, the relative amplitude $|\delta r_p|/R_p$ of the ϕ variation of the radial payload displacement by the end of the implosion at $t = t_{im}$ in Eq. (9) will be of the order of $\bar{\nu}^{-2}$—even when

calculated with the full account for the retardation effect. Hence, the square-root dependence on C_r for smooth pulses in Eq. (17) is retained even when $t_b \simeq t_{im}$.

B. Focal nonuniformities

Here we analyze the role of focal nonuniformities for an elliptical beam ($a_f \neq b_f$; see Fig. 1), which preserves its orientation during the rotation along a circular orbit $r=R_b$. Such a case corresponds to the quadrupole asymmetry of the energy deposition and implosion pattern.

Under the same simplifying assumptions as for the cyclic nonuniformities, namely, that (i) the payload and the absorber are thin compared to their radii and (ii) the pulse duration t_b is short compared to the implosion time t_{im}, and having supposed in addition that (iii) the rotation frequency ν is so large that the cyclic nonuniformities are negligibly small, we can use the self-similar solution from Appendix A to evaluate the ensuing quadrupole asymmetry of the radial displacement of the gas-payload interface. Under our assumptions, this distance is

$$R_p - r_p(t_{im},\phi) = Y(t_{im}) - Y_0 \approx Y(t_{im}) \propto \left(\frac{\epsilon_{\mathrm{tot}}}{\mu_{pa} + \frac{1}{3}} \right)^{1/2}, \tag{19}$$

where $\frac{1}{2}\mu_{pa}$ is the mass ratio between the payload and the absorber. Then, for the azimuthal relative nonuniformity of the radial displacement we obtain

$$\frac{\delta r_p}{R_p} = -\frac{1}{2}\frac{\delta \epsilon_{\mathrm{tot}}}{\epsilon_{\mathrm{tot}}} + \frac{1}{2}\frac{\delta \mu_{pa}}{\mu_{pa} + \frac{1}{3}}. \tag{20}$$

Note that, in contrast to the cyclic nonuniformities, now the azimuthal variations of the travelled distance arise not only from the variations in the energy deposition but also from the variations of the payload areal mass m_p.

Having defined $\delta\epsilon_{\mathrm{tot}}$ for the quadrupole perturbation as $\epsilon_{\mathrm{tot}}(0) - \epsilon_{\mathrm{tot}}(\pi/2)$, we readily obtain

$$\frac{\delta \epsilon_{\mathrm{tot}}}{\epsilon_{\mathrm{tot}}} = \delta_f, \tag{21}$$

where δ_f is defined in Eq. (2). Assuming the same initial density for the absorber and the payload, we have a ϕ independent value of the sum $m_a + m_p$, which leads to

$$\delta\mu_{pa} = \frac{\delta m_p}{m_a} - \mu_{pa}\frac{\delta m_a}{m_a} = -\frac{\delta m_a}{m_a}(1+\mu_{pa}) = \delta_f(1+\mu_{pa}). \tag{22}$$

Because $\delta\epsilon_{\mathrm{tot}}$ and $\delta\mu_{pa}$ have the same sign, the two terms on the right-hand side (rhs) of Eq. (20) partially cancel one another. The physical cause of this compensation is quite clear: where the distorted focal spot sweeps a more narrow absorber band (Fig. 1), the specific energy deposition ϵ_{tot} increases together with the payload/absorber mass ratio $m_p/(2m_a) = \frac{1}{2}\mu_{pa}$. In our case the effect of the heavier payload prevails, and Eqs. (20), (21), and (22) yield

$$\frac{|\delta r_p|}{R_p} = \frac{|\delta_f|}{1+3\mu_{pa}}. \tag{23}$$

Then, having recalled Eq. (9), we arrive at the following constraint on the value of $|\delta_f|$:

$$|\delta_f| \leqslant \frac{1+3\mu_{pa}}{\sqrt{2}\, C_r}. \tag{24}$$

Equation (24) tells us that, beside the radial convergence C_r, the impact of focal nonuniformities is sensitive also to the relative payload mass μ_{pa}. As it will be seen from the numerical simulations, other parameters (like pulse duration, absorber thickness) are of importance as well.

IV. NUMERICAL SIMULATIONS

Numerical simulations have been performed with the 2D arbitrary Lagrangian–Eulerian hydrodynamics code CAVEAT[11] in the (r,ϕ) cylindrical geometry. For the present problem, the heat conduction was ignored. We used a simple linear equation of state (EOS)

$$p = p(\rho,e) = c_0^2(\rho - \rho_0) + \Gamma\rho e, \tag{25}$$

where p, ρ, and e are, respectively, the pressure, the density, and the specific internal energy, and c_0, ρ_0, and Γ are constants: c_0 is the sound speed at normal density $\rho=\rho_0$ and zero internal energy $e=0$ (zero pressure), Γ is the Grüneisen coefficient. The caloric EOS (25) has an important advantage that it admits an equivalent analytic representation in the more familiar thermal form,

$$\begin{aligned} p &= p(\rho,T) = p_c(\rho) + \Gamma\rho c_v T, \\ e &= e(\rho,T) = e_c(\rho) + c_v T, \end{aligned} \tag{26}$$

where T is the temperature, and the cold pressure p_c and specific energy e_c are given by

$$\begin{aligned} p_c(\rho) &= \frac{\rho_0 c_0^2}{\Gamma+1}\left[\left(\frac{\rho}{\rho_0} \right)^{\Gamma+1} - 1 \right], \\ e_c(\rho) &= c_0^2\left[\frac{1}{\Gamma(\Gamma+1)}\left(\frac{\rho}{\rho_0} \right)^{\Gamma} + \frac{1}{\Gamma+1}\frac{\rho_0}{\rho} - \frac{1}{\Gamma} \right], \end{aligned} \tag{27}$$

here $c_v > 0$ is a physically insignificant additional constant (specific heat at constant volume), whose value is fully determined by the temperature unit. Expressions (27) are obtained by excluding T from two Eqs. (26), combining the result with the basic thermodynamic identity $\rho^2\, de_c/d\rho = p_c$, and performing elementary integration. Equation (26) belongs to the well known class of two-term equations of state[10] that are quite adequate for compressed metals at not too high energy densities. For $c_0=0$ it reduces to the ideal-gas EOS with the adiabatic index $\gamma = \Gamma + 1$.

For $c_0 > 0$, $\rho_0 > 0$ our EOS has a useful property that the density at a boundary with vacuum is always finite, which is characteristic for liquid metals, and which prevents our target from disassembly before a significant amount of energy is deposited. On the other hand, this EOS has an unphysical property that the internal energy becomes infinite at $\rho=0$. However, in the simulations we never reached states where such unphysical behavior could become of any importance. We used the values $c_0=0$, $\Gamma=2/3$ to describe the central gas (initially at $r<R_p$), and the values

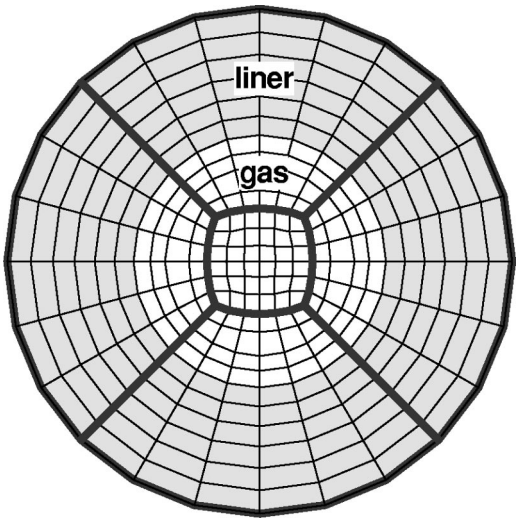

FIG. 3. Schematic view of the numerical mesh, consisting of five separate blocks, that was used in 2D hydrodynamic simulations. Thick lines show the boundaries between blocks.

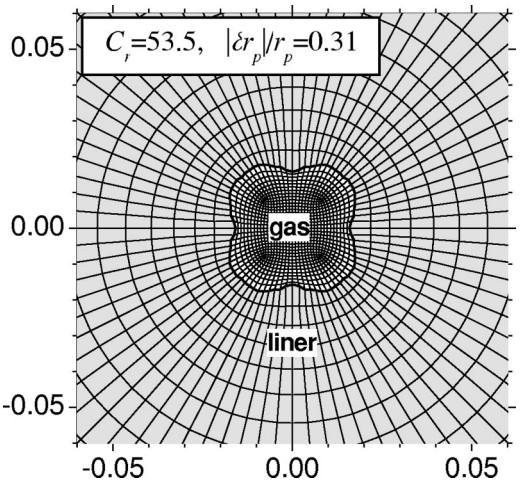

FIG. 4. Configuration of the central gas region at the time of stagnation in a test run with an azimuthally symmetric beam energy deposition. The initial position of the liner-gas interface was at $r=R_p=1$.

$$\rho_0=10\ \text{g/cm}^3,\quad c_0=2.5\times10^5\ \text{cm/s},\quad \Gamma=2.5, \tag{28}$$

for the solid liner shell. The values (28) correspond roughly to the properties of lead near normal conditions.[10]

A special routine has been added to the original CAVEAT code to describe the energy deposition by a rotating ion beam. For the spatial beam current profile, we assumed an inverted parabolic distribution over an elliptical focal spot with semiaxes a_f and b_f (see Fig. 1). The specific heating rate [W/g] at a given point (x,y) of the target cross section has been calculated as

$$q(t,x,y)=\frac{2W_b(t)}{\pi a_f b_f \mathcal{R}}\left(1-\frac{x_f^2}{a_f^2}-\frac{y_f^2}{b_f^2}\right), \tag{29}$$

where

$$x_f=x-R_b\sin(2\pi\nu t),$$
$$y_f=y-R_b\cos(2\pi\nu t), \tag{30}$$

are local coordinates with respect to the center of the rotating focal ellipse. Outside the focal ellipse, i.e., for $|x_f|>a_f$ or $|y_f|>b_f$, the heating rate $q(t,x,y)$ is equal to zero. For each quadrangular mesh cell, the heating rate (29) was numerically integrated over the cell area by using a Gaussian quadrature with 2–5 nodes along each spatial direction, and analytically integrated over the time interval $[t,t+\Delta t]$, where Δt is the current hydrodynamic time step. Such a procedure allowed us to avoid any restrictions on Δt due to fast beam rotation.

To simulate a circular cross section of a cylindrical target, we used a numerical mesh shown in Fig. 3. This mesh consists of five separate blocks and has a floating center. The central block has the topology of a square. Such a mesh has two important advantages over a simple radial (r,ϕ) mesh with a fixed center at $r=0$: (i) it allows the central gas region to be pushed aside in the course of an asymmetric implosion without problems with rezoning and (ii) it is less restrictive with respect to the Courant limit on the time step.

On the other hand, our mesh has a serious shortcoming of being initially not perfectly symmetric with respect to ϕ rotation, which inevitably leads to spurious ϕ perturbations at sufficiently high radial convergences even for a perfectly symmetric beam heating. Special tests have shown, however, that this defect is not harmful to our problem, provided that the initial radius of the central block is set to be sufficiently small [in practice, the values of $(0.2-0.3)R_p$ were used]. Figure 4 shows the liner-gas interface in such a test run with a perfectly symmetric beam energy deposition at the time of stagnation, when essentially the 1D convergence ratio of $C_r=53.5$ has been reached. What is important, the relative deformation $|\delta r_p|/r_p=0.31$ of the liner-gas interface [as defined in Eq. (32)] is still well below the critical value of 1.

A. Cyclic nonuniformities

To explore the effect of cyclic nonuniformities, the base series of simulations has been conducted for the following set of parameters:

$$R_p=1\ \text{mm},\quad R_b=1.55\ \text{mm},\quad R=2.55\ \text{mm},$$
$$a_f=b_f=r_f=0.5\ \text{mm}, \tag{31}$$
$$E_b=20\ \text{kJ},\quad t_b=200\ \text{ns},\quad \mathcal{R}=10\ \text{g/cm}^2.$$

These parameters correspond to the mean total energy deposition of $E_b/(S_a\mathcal{R})=20.5$ kJ/g, and result in the implosion time of $t_{im}\approx t_b$. The effective range of 10 g/cm^2 corresponds to the stopping power of lead for the uranium ions with the energy of 0.5 GeV per nucleon. The initial density ρ_{g0} of the central gas was set sufficiently low, typically between 10^{-4} g/cm^3 and 2×10^{-3} g/cm^3, so that to exclude the impact of the counterpressure of the compressed central gas on the distortion of the liner-gas interface; in other words, the 1D convergence ratio corresponding to the limit of $\overline{\nu}\to\infty$ was kept always significantly higher than the final 2D value for a given finite $\overline{\nu}$. The initial target pressure was close to zero (1 bar).

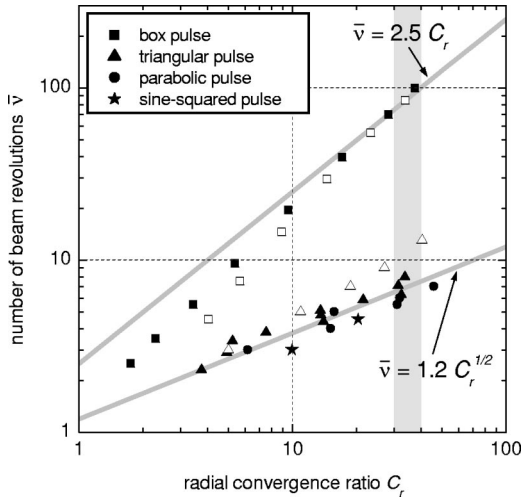

FIG. 5. Results of 2D simulations for cyclic nonuniformities: the lower bound on the number of beam revolutions $\bar{\nu}$ is plotted versus the desired value of the radial convergence ratio C_r for the base set of target parameters (31) and four different pulse shapes (8). Filled symbols correspond to $t_b = 200$ ns, open symbols correspond to $t_b = 2$ ns.

In each simulation we kept track of the Lagrangian interface $r_p(t,\phi)$ between the liner and the central gas. Each simulation was terminated whenever the relative distortion of this interface, defined as

$$\frac{|\delta r_p|}{r_p} = \frac{\max_\phi\{r_p(t,\phi)\} - \min_\phi\{r_p(t,\phi)\}}{\sqrt{S_g/\pi}}, \tag{32}$$

exceeded unity; here $S_g = S_g(t)$ is the surface area inside the closed curve $r = r_p(t,\phi)$. Note that thus defined distortion may become large not only due to a noncircular shape of the gas-liner interface, but also due to a significant displacement of the circular interface from its original position. Typically, we used 120 mesh points over the 360 degrees of the ϕ direction, and about 100 mesh points in radial direction. Check runs with 240 intervals in ϕ have produced practically identical results.

The results of simulations for the base set of parameters are shown in Fig. 5 with filled symbols. For each symbol, the abscissa is the convergence ratio C_r—as calculated from Eq. (4)—reached by the final time when $|\delta r_p|/r_p = 1$, and the ordinate is the number of beam revolutions $\bar{\nu}$ over the pulse duration t_b. Considering the values $C_r = 30-40$ as an upper limit on realistic values of the radial convergence, we did not pursue our simulations beyond this range (shown as a gray vertical band in Fig. 5). Symbols of different shape represent different pulse shapes.

Figure 5 clearly demonstrates that for all the smooth pulses (including the sine-squared pulse) our 2D simulations fully confirm the analytical estimate (17). Within the scatter of numerical results, even the coefficient in Eq. (17) agrees with the simulations. Recall that the estimate (17) has been obtained under the assumptions of $t_b \ll t_{im}$ and of a thin absorber+payload layer, both of which are not satisfied by the parameter set (31).

The case of the sine-squared pulse deserves a special comment. This pulse has zero time derivatives at both ends,

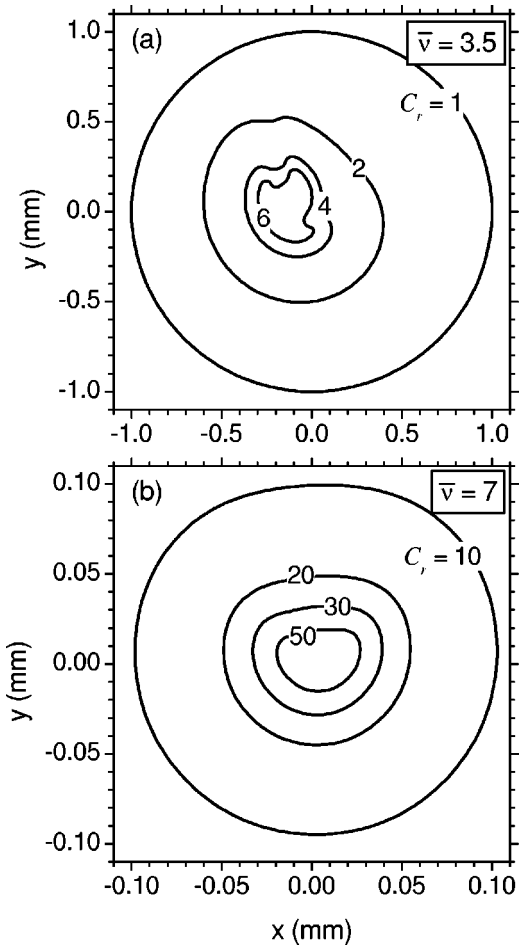

FIG. 6. Evolution of the liner-gas interface in two different cases: (a) $\bar{\nu} = 3.5$ beam revolutions with a box pulse shape; (b) $\bar{\nu} = 7$ beam revolutions with a smooth parabolic pulse shape. Each curve is marked by the corresponding current value of the convergence ratio C_r.

$\Omega'(0) = \Omega'(1) = 0$, and, as it follows from Eq. (16), should produce $|\delta\epsilon_{\rm tot}|/\epsilon_{\rm tot} \propto \bar{\nu}^{-3}$, hence $\bar{\nu} \propto C_r^{1/3}$ in Fig. 5. This is not observed simply because the total number of revolutions ($\simeq 6$) required to reach $C_r = 30$ is still too low: the expansion of $|\delta\epsilon_{\rm tot}|/\epsilon_{\rm tot}$ in powers of $\bar{\nu}^{-1}$ becomes sufficiently accurate only when the revolution period is shorter than all characteristic time scales for variation of all relevant derivatives. Thus, from the practical point of view it hardly makes any sense to try to generate power pulses with zero first and higher time derivatives at pulse ends.

For the box pulse, the 2D simulations produce significantly worse results than predicted by Eq. (17): not only the numerical coefficient in the inferred constraint $\bar{\nu} \gtrsim 2.5 C_r$ turns out to be about a factor 3 higher than in Eq. (17), but the required number of beam revolutions $\bar{\nu}$ grows somewhat faster than in direct proportion with C_r. The latter is, most likely, caused by the fact that a sudden power rise generates a short-scale (along the ϕ direction) perturbation in the velocity field, which quickly becomes nonlinear. This is clearly seen in Fig. 6(a), where the evolution of the gas-liner interface is shown as a function of the radial convergence C_r for a box pulse with $\bar{\nu} = 3.5$ beam revolutions. For comparison, Fig. 6(b) shows the evolution of this same interface for a

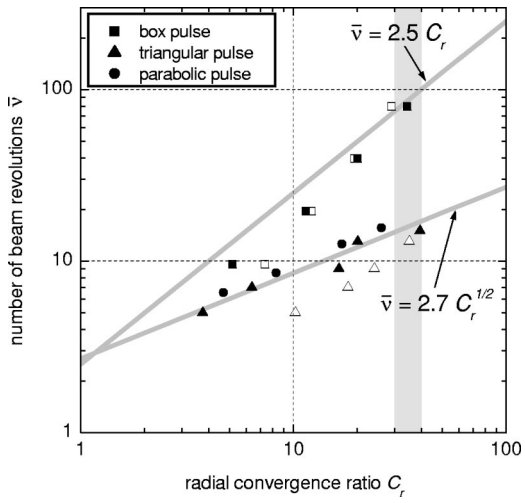

FIG. 7. Same as Fig. 5 but for a set of target parameters (33) with a relatively thin absorber. Filled symbols correspond to $t_b = 50$ ns, open symbols correspond to $t_b = 0.5$ ns.

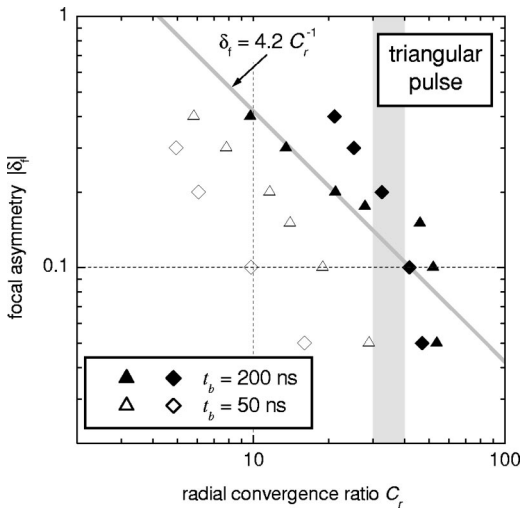

FIG. 8. Results of 2D simulations for focal nonuniformities: the upper bound $|\delta_f|$ on the asymmetry of the focal spot is plotted versus the desired value of the radial convergence ratio C_r for a triangular pulse with $\bar{\nu} = 9$ beam revolutions and the base set of target parameters (31) with two different values of the beam orbit: $R_b = 1.55$ mm (triangles) and $R_b = 1.65$ mm (diamonds). Filled symbols correspond to $t_b = 200$ ns, open symbols correspond to $t_b = 50$ ns.

much more symmetric case with seven beam revolutions over the parabolic pulse profile.

To explore the role of retardation, we have conducted two additional series of simulations (for the box and the triangular pulses) with a very short pulse duration of $t_b = 2$ ns but all the other parameters from Eq. (31) unchanged. The results are plotted in Fig. 5 with open squares and triangles. Now, with the implosion time of $t_{im} \approx 100$ ns, the dimensionless parameter $t_b/t_{im} \approx 0.02$ is close to zero and the retardation effect is practically excluded. However, the situation is complicated by the fact that the regime of the payload acceleration is also changed from the slow quasiadiabatic to the fast shock-like one. If we recall that the analytical estimate (17) was based on the assumption of quasiadiabatic payload acceleration, which breaks down for short pulses, it becomes no surprise that the open squares and triangles (in both Fig. 5 and Fig. 7) exhibit noticeable deviations from the $\bar{\nu} \propto C_r$ and $\bar{\nu} \propto C_r^{1/2}$ laws. Fortunately, the final results turn out to be not particularly sensitive to such extreme variations of the pulse duration t_b, and our conclusions, as formulated in Eq. (34) below, apply to the entire range of realistic values of the beam pulse duration t_b.

To check the other simplifying assumption behind the analytical result (17), namely that of a thin absorber ($r_f \ll R_b$), we have repeated the simulations shown in Fig. 5 for a five times thinner absorber, namely, for a combination of parameters,

$$R_p = 1 \text{ mm}, \quad R_b = 1.15 \text{ mm}, \quad R = 1.75 \text{ mm},$$
$$a_f = b_f = r_f = 0.1 \text{ mm}, \tag{33}$$
$$E_b = 100 \text{ kJ}, \quad t_b = 50 \text{ ns}, \quad \mathcal{R} = 10 \text{ g/cm}^2.$$

A five times higher than in Eq. (31) value of E_b has been chosen to avoid unphysical thermodynamic properties of a highly expanded absorber, obeying the equation of state (25), at a not high enough specific energy deposition. The results of simulations are shown in Fig. 7. Similar to Fig. 5, filled symbols correspond to $t_b/t_{im} \approx 1$ (now the implosion time $t_{im} \approx 60$ ns), while empty squares and triangles correspond to $t_b/t_{im} \approx 0.03$. It is seen that we obtain practically the same as in Fig. 5 results for both cases of the box pulse and for the short triangular pulse. However, long smooth pulses require now about two times larger number of beam revolutions to achieve the same convergence ratio C_r. Qualitatively, this can be explained by the fact that in targets with relatively thinner absorbers the implosion proceeds relatively faster with respect to the propagation of pressure waves along the ϕ direction, which tend to smooth out the pressure perturbations generated by the nonuniform energy deposition. Finally note that the two sets (31) and (33) differ also in the value of the absorber-payload mass ratio μ_{pa}. A series of dedicated code runs has shown, however, that the lower bound on $\bar{\nu}$ is insensitive to this parameter.

B. Focal nonuniformities

In contrast to the cyclic perturbations, the impact of focal nonuniformities on the symmetry of implosion is insensitive to the temporal beam power profile. Figure 8 shows the results of 2D simulations in terms of the focal asymmetry $|\delta_f|$ as a function of the convergence ratio C_r that can be reached for given $|\delta_f|$. These results have been obtained for the triangular pulse (8) with $\bar{\nu} = 9$ beam revolutions by fixing the vertical semiaxis of the rotating focal ellipse at $b_f = 0.5$ mm and varying its horizontal semiaxis within the range $0.34 \text{ mm} \leqslant a_f \leqslant 0.5$ mm. Filled triangles correspond to the base set of target parameters (31), while open triangles have been obtained for a pulse duration shortened from 200 ns to $t_b = 50$ ns. These simulations confirm that in general the upper bound on $|\delta_f|$ is inversely proportional to C_r, although the proportionality coefficient may differ significantly from the analytical estimate (24).

Equation (24) tells us that, apart from C_r, the constraint on $|\delta_f|$ depends also on the relative payload mass μ_{pa}. To check this dependence, we have conducted a series of simulations with a thicker than in Eq. (31) payload (filled and open diamonds in Fig. 8) by shifting the beam orbit from $R_b=1.55$ mm to $R_b=1.65$ mm, which allowed us to increase the parameter μ_{pa} from $\mu_{pa}\approx 0.27$ to $\mu_{pa}\approx 0.37$. It is seen that, in qualitative agreement with Eq. (24), the upper bound on $|\delta_f|$ does indeed increase with μ_{pa}—but only for a long pulse with $t_b=200$ ns. For shorter pulses with $t_b=50$ ns the dependence on μ_{pa} is just the opposite. Such a behavior is caused by the change of the regime of the payload acceleration (from the quasiadiabatic to the shock-like one) as we reduce the beam pulse duration t_b. Our simulations clearly demonstrate that the quadrupole asymmetry of the payload-gas interface even changes sign (from oblate to prolate) as we keep $a_f<b_f$ fixed and change the pulse duration from $t_b=200$ ns to $t_b=50$ ns. Finally, the main conclusion from Fig. 8 is that, unlike the cyclic perturbations, the effect of focal nonuniformities is quite sensitive to the target parameters and to the ion pulse duration.

V. CONCLUSION

We have investigated the symmetry of cylindrical implosions driven by an intense beam of fast ions, which propagates along the axis of a cylindrical target and, simultaneously, rotates around this same axis. Two types of azimuthal nonuniformities have been analyzed both analytically and in 2D hydrodynamic simulations.

Cyclic nonuniformities, caused by the finite number of beam revolutions, are found to be sensitive to the temporal beam power profile. According to our calculations, the lower bound on the required cyclic frequency ν of the beam wobbler, expressed in terms of the total number of the beam revolutions $\overline{\nu}$ during the pulse, can be written as

$$\overline{\nu}\gtrsim\begin{cases}2.5C_r, & \text{box pulse,}\\ (1-3)C_r^{1/2}, & \text{smooth pulse,}\end{cases} \tag{34}$$

where C_r is the desired radial convergence ratio of the implosion. A given pulse shape should be classified either as a box pulse or as a smooth pulse depending on whether the beam power experiences sudden changes on a time scale shorter than the beam rotation period ν^{-1}, or varies smoothly on a time scale of the total pulse duration t_b. The uncertainty in the numerical factor for smooth pulses reflects sensitivity of the cyclic nonuniformities to the target geometry and the ion pulse duration. The most lenient constraints on $\overline{\nu}$ are obtained for smooth pulses when the focal radius r_f of the rotating beam is relatively large (i.e., comparable to the radius of the beam orbit R_b), and the pulse duration t_b is relatively long (i.e., comparable to the implosion time t_{im}).

Focal nonuniformities, caused by a noncircular ion current distribution over the focal spot of a rotating beam, have been investigated for an example of the elliptical focal spot. In general, the upper bound on the ellipticity $|\delta_f|$ of the focal spot is inversely proportional to the radial convergence ratio C_r, but the proportionality coefficient varies in a broad range depending on the target proportions and the ion pulse duration. The temporal shape of the irradiating pulse is relatively unimportant. Targets with relatively thick absorber and payload layers, irradiated by relatively long pulses, can tolerate as large as a 20% asymmetry of the focal spot and still demonstrate convergence ratios $C_r\gtrsim 30$. In practice, however, the role of the focal nonuniformities should be analyzed individually for each combination of the target and beam parameters.

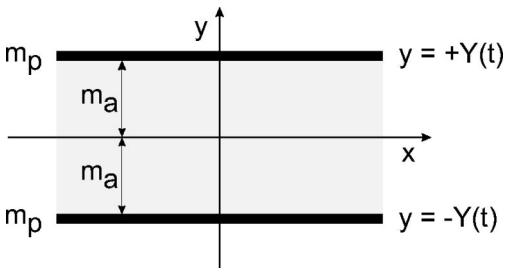

FIG. 9. A planar absorber-payload slab symmetric with respect to the $y=0$ plane.

ACKNOWLEDGMENTS

One of the authors (M.M.B.) is grateful to the staff of the Institut für Kernphysik at TU Darmstadt, to Professor D. H. H. Hoffmann, and to all members of his group at the Gesellschaft für Schwerionenforschung (Darmstadt) for providing an office space, friendly assistance, and many stimulating discussions during his three-month stay at the GSI–TU Darmstadt.

APPENDIX A: SELF-SIMILAR SOLUTION FOR A QUASIADIABATIC ACCELERATION OF THE PAYLOAD BY A UNIFORMLY EXPANDING ABSORBER

Consider a uniform plane-parallel absorber layer at $-Y(t)\leqslant y\leqslant Y(t)$ (see Fig. 9), which is symmetric with respect to the plane $y=0$ and has two infinitely thin payload sheets on each side at $y=\pm Y(t)$; each payload sheet has a finite areal mass of m_p [$\mathrm{g\,cm^{-2}}$]. To obtain an analytic solution, we use the ideal-gas equation of state

$$e=\frac{1}{\gamma-1}\frac{p}{\rho}, \tag{A1}$$

for the absorber fluid and write down the 1D hydrodynamic equations in the Lagrangian form

$$\frac{\partial y}{\partial t}=u, \tag{A2}$$

$$\frac{\partial u}{\partial t}+\frac{\partial p}{\partial m}=0, \tag{A3}$$

$$\frac{\partial e}{\partial t}+p\frac{\partial u}{\partial m}=q(t,m), \tag{A4}$$

with respect to the mass coordinate

$$-m_a\leqslant m=\int_0^y \rho(t,y')dy'\leqslant m_a, \tag{A5}$$

where u, ρ, p, and e are, respectively, the velocity, the density, the pressure, and the specific (per unit mass) energy of the absorber fluid, $m_a=\int_0^Y \rho(t,y')dy'$ is one-half of the absorber areal mass, $q(t,m)$ [$\mathrm{erg\,g^{-1}\,s^{-1}}$] is the specific (per unit mass) rate of the energy deposition.

Equations (A2)–(A4) admit a simple homologous [i.e., with a uniform density, $\rho(t,m)=\rho(t)=m_a/Y(t)$, and a linear velocity, $u(t,y)\propto y$, profiles] self-similar solution

$$y(t,m)=\xi Y, \quad u(t,m)=\xi\dot{Y}, \tag{A6}$$

$$p(t,m)=m_a\ddot{Y}[\mu_{pa}+\tfrac{1}{2}(1-\xi^2)], \tag{A7}$$

$$e(t,m)=\frac{p}{(\gamma-1)\rho}=\frac{Y\ddot{Y}}{\gamma-1}\left[\mu_{pa}+\frac{1}{2}(1-\xi^2)\right], \tag{A8}$$

provided that the specific heating rate $q(t,m)$ has a parabolic profile

$$q(t,m)=q_a(t)[\mu_{pa}+\tfrac{1}{2}(1-\xi^2)][\mu_{pa}+\tfrac{1}{3}]^{-1} \tag{A9}$$

with respect to the mass coordinate m; here

$$\xi=\frac{m}{m_a} \tag{A10}$$

is the self-similar variable, $\mu_{pa}=m_p/m_a$ is the dimensionless pusher mass, $\dot{Y}$ and $\ddot{Y}$ are the first and the second derivatives of $Y(t)$, and $q_a(t)$ is an arbitrary given mean heating rate (averaged over the absorber thickness, so that $2m_aq_a$ [$\mathrm{erg\,cm^{-2}\,s^{-1}}$] is the heating rate per unit area of the absorber-payload slab) of the absorber. For a given $q_a(t)$, the function $Y(t)$ is found by solving the ordinary differential equation

$$\frac{Y\ddot{Y}}{\gamma-1}+\frac{1}{2}\dot{Y}^2=\frac{\epsilon(t)}{\mu_{pa}+\frac{1}{3}} \tag{A11}$$

with the initial conditions

$$Y(0)=Y_0=\frac{m_a}{\rho_{a0}}, \quad \dot{Y}(0)=0, \tag{A12}$$

where

$$\epsilon(t)=\int_0^t q_a(t')dt' \tag{A13}$$

is the mean specific deposited energy, ρ_{a0} is the initial absorber density. Here we assume that the initial internal and kinetic energies of the absorber-payload slab are zero. Note that for $\xi=1$ Eq. (A7) describes the acceleration of the payload,

$$p(t,m_a)=m_p\ddot{Y}. \tag{A14}$$

Equation (A11) can be explicitly integrated in the specific case of $\gamma=3$,

$$Y^2(t)=Y_0^2+\frac{4}{\mu_{pa}+\frac{1}{3}}\int_0^t\left[\int_0^{t'}\epsilon(t'')dt''\right]dt'. \tag{A15}$$

This solution becomes particularly simple in the limiting case of a very fast energy deposition, $q_a(t)=\epsilon_{\mathrm{tot}}\delta(t)$:

$$Y^2(t)=Y_0^2+\frac{2\epsilon_{\mathrm{tot}}}{\mu_{pa}+\frac{1}{3}}t^2. \tag{A16}$$

APPENDIX B: NONUNIFORMITY OF THE TOTAL SPECIFIC ENERGY DEPOSITION FOR DIFFERENT PULSE SHAPES

When normalized to its ϕ-averaged value of $E_b/(S_a\mathcal{R})$, the mean (over the radial absorber thickness) total specific energy deposition in a thin absorber, given by Eqs. (11) and (12) for $t=t_b$, can be rewritten as

$$\omega(\phi,\overline{\nu})\equiv\frac{\epsilon_{\mathrm{tot}}(\phi,\nu)}{E_b/(S_a\mathcal{R})}=\frac{1}{\overline{\nu}}\sum_{k=1}^{N}\Omega(\tau_k), \tag{B1}$$

where

$$\tau_k=\frac{1}{\overline{\nu}}\left(\frac{\phi}{2\pi}+k-1\right),$$
$$N=\begin{cases}[\overline{\nu}]+1, & 0\leqslant\dfrac{\phi}{2\pi}<\Delta\overline{\nu}\leqslant 1,\\[2ex] [\overline{\nu}], & \Delta\overline{\nu}\leqslant\dfrac{\phi}{2\pi}<1,\end{cases} \tag{B2}$$

$[\overline{\nu}]$ is the integer part of $\overline{\nu}$, and $\Delta\overline{\nu}=\overline{\nu}-[\overline{\nu}]$ is the fractional part of $\overline{\nu}$. Clearly, for large $\overline{\nu}\gg 1$ the dimensionless function $\omega(\phi,\overline{\nu})$ is close to 1, and the angular nonuniformity of the total deposited energy is simply

$$\frac{|\delta\epsilon_{\mathrm{tot}}|}{\epsilon_{\mathrm{tot}}}=\max_{\phi}\{\omega(\phi,\overline{\nu})\}-\min_{\phi}\{\omega(\phi,\overline{\nu})\}. \tag{B3}$$

In the simplest case of a box-like pulse, when $\Omega(\tau)=1$, calculation of $\omega(\phi,\overline{\nu})$ is trivial, and the result is

$$\omega(\phi,\overline{\nu})=\begin{cases}\dfrac{[\overline{\nu}]+1}{\overline{\nu}}, & 0\leqslant\dfrac{\phi}{2\pi}<\Delta\overline{\nu},\\[2ex] \dfrac{[\overline{\nu}]}{\overline{\nu}}, & \Delta\overline{\nu}\leqslant\dfrac{\phi}{2\pi}<1.\end{cases} \tag{B4}$$

Equations (B3) and (B4) yield Eq. (14).

1. Triangular power pulse

In the case of a triangular pulse with $\Omega(\tau)=2(1-|2\tau-1|)$, the summation in Eq. (B1) can be also done exactly. For even values of $[\overline{\nu}]$ we find

$$\omega(\phi,\overline{\nu})=1-\frac{\Delta\overline{\nu}^2}{\overline{\nu}^2}+\frac{4}{\overline{\nu}^2}$$
$$\times\begin{cases}\dfrac{\phi}{2\pi}, & 0\leqslant\dfrac{\phi}{2\pi}\leqslant\dfrac{1}{2}\Delta\overline{\nu},\\[2ex] \left(\Delta\overline{\nu}-\dfrac{\phi}{2\pi}\right), & \dfrac{1}{2}\Delta\overline{\nu}<\dfrac{\phi}{2\pi}\leqslant\Delta\overline{\nu},\\[2ex] 0, & \Delta\overline{\nu}\leqslant\dfrac{\phi}{2\pi}\leqslant 1,\end{cases} \tag{B5}$$

and for odd $[\overline{\nu}]$ we obtain

$$\omega(\phi,\overline{\nu})=1-\frac{(1-\Delta\overline{\nu})^2}{\overline{\nu}^2}+\frac{4}{\overline{\nu}^2}\times\begin{cases}0, & 0\leqslant\dfrac{\phi}{2\pi}\leqslant\Delta\overline{\nu},\\ \left(\dfrac{\phi}{2\pi}-\Delta\overline{\nu}\right), & \Delta\overline{\nu}<\dfrac{\phi}{2\pi}\leqslant\dfrac{1}{2}(1+\Delta\overline{\nu}),\\ \left(1-\dfrac{\phi}{2\pi}\right), & \dfrac{1}{2}(1+\Delta\overline{\nu})\leqslant\dfrac{\phi}{2\pi}\leqslant 1.\end{cases}\quad\text{(B6)}$$

Equations (B5) and (B6) yield Eq. (15) for the full amplitude of the ϕ variations of $\omega(\phi,\overline{\nu})$.

2. Arbitrary smooth pulse

For an arbitrary smooth pulse we assume that the pulse profile $\Omega(\tau)$ has the first, $\Omega'(\tau)$, and the second, $\Omega''(\tau)$, derivatives in the interval $0<\tau<1$. Being interested in large values of $\overline{\nu}\gg 1$, we can expand the function $\omega(\phi,\overline{\nu})$ in a power series with respect to the small parameter $\overline{\nu}^{-1}$ and retain the first nonvanishing nontrivial term. Before doing so, we note that Eq. (B1) is nothing else but a trapezoidal-rule quadrature formula for numerical integration of the function $\Omega(\tau)$ on a uniform mesh $\{\tau_i\}=\{0;\overline{\nu}^{-1};2\overline{\nu}^{-1};3\overline{\nu}^{-1},\ldots\}$. For any continuous function $\Omega(\tau)$, the error of such numerical quadrature is of the order of $\overline{\nu}^{-2}$, i.e., we expect that $\omega(\phi,\overline{\nu})=1+O(\overline{\nu}^{-2})$.

First consider the case of $0\leqslant\phi/2\pi<\Delta\overline{\nu}$, when $N=[\overline{\nu}]+1$. We start with the identity

$$1=\int_0^1\Omega(\tau)d\tau=\sum_{k=1}^{\overline{\nu}}\int_{(k-1)/\overline{\nu}}^{k/\overline{\nu}}\Omega(\tau)d\tau+\int_{[\overline{\nu}]/\overline{\nu}}^1\Omega(\tau)d\tau,\quad\text{(B7)}$$

in which we perform a piecewise Taylor series expansion,

$$\Omega(\tau)=\Omega_k+(\tau-\tau_k)\Omega_k'+\frac{1}{2}(\tau-\tau_k)^2\Omega_k''+\cdots,\qquad\frac{k-1}{\overline{\nu}}<\tau<\frac{k}{\overline{\nu}},\quad\text{(B8)}$$

and calculate

$$\int_{(k-1)/\overline{\nu}}^{k/\overline{\nu}}\Omega(\tau)d\tau=\frac{\Omega_k}{\overline{\nu}}+\frac{\Omega_k'}{2\overline{\nu}^2}\left(1-\frac{\phi}{\pi}\right)+\frac{\Omega_k''}{6\overline{\nu}^3}\left[1-\frac{3\phi}{2\pi}+3\left(\frac{\phi}{2\pi}\right)^2\right]+\cdots,\quad k=1,2,\ldots,[\overline{\nu}],\quad\text{(B9)}$$

$$\int_{[\overline{\nu}]/\overline{\nu}}^1\Omega(\tau)d\tau=\frac{\Omega_N}{\overline{\nu}}\Delta\overline{\nu}+\frac{\Omega_N'}{2\overline{\nu}^2}\Delta\overline{\nu}\left(\Delta\overline{\nu}-\frac{\phi}{\pi}\right)+\frac{\Omega_N''}{6\overline{\nu}^3}\times\Delta\overline{\nu}\left[\Delta\overline{\nu}^2-\Delta\overline{\nu}\frac{3\phi}{2\pi}+3\left(\frac{\phi}{2\pi}\right)^2\right]+\cdots,\quad\text{(B10)}$$

where $\Omega_k=\Omega(\tau_k)$, $\Omega_k'=\Omega'(\tau_k)$, $\Omega_k''=\Omega''(\tau_k)$. Having substituted Eqs. (B9) and (B10) into Eq. (B7), we obtain

$$1=\omega(\phi,\overline{\nu})-\frac{1}{\overline{\nu}}(1-\Delta\overline{\nu})\Omega_N+\frac{1}{2\overline{\nu}^2}\left(1-\frac{\phi}{\pi}\right)\sum_{k=1}^{[\overline{\nu}]}\Omega_k'+\frac{1}{6\overline{\nu}^3}\left[1-\frac{3\phi}{2\pi}+3\left(\frac{\phi}{2\pi}\right)^2\right]\sum_{k=1}^{[\overline{\nu}]}\Omega_k''+\frac{\Delta\overline{\nu}}{2\overline{\nu}^2}\left(\Delta\overline{\nu}-\frac{\phi}{\pi}\right)\Omega_N'+\cdots,\quad\text{(B11)}$$

here and below we omit all the terms of the order of $\overline{\nu}^{-3}$ and higher. To evaluate $\Sigma_{k=1}^{[\overline{\nu}]}\Omega_k'$, we note that, analogously to Eqs. (B7) and (B11),

$$0=\int_0^1\Omega'(\tau)d\tau=\frac{1}{\overline{\nu}}\sum_{k=1}^{[\overline{\nu}]}\Omega_k'+\frac{1}{2\overline{\nu}^2}\left(1-\frac{\phi}{\pi}\right)\sum_{k=1}^{[\overline{\nu}]}\Omega_k''+\frac{\Delta\overline{\nu}}{\overline{\nu}}\Omega_N'+\cdots,\quad\text{(B12)}$$

which yields

$$\sum_{k=1}^{[\overline{\nu}]}\Omega_k'=-\frac{1}{2\overline{\nu}}\left(1-\frac{\phi}{\pi}\right)\sum_{k=1}^{[\overline{\nu}]}\Omega_k''-\Delta\overline{\nu}\Omega_N'+\cdots.\quad\text{(B13)}$$

Also, the same reasoning leads to

$$\int_0^1\Omega''(\tau)d\tau=\Omega'(1)-\Omega'(0)=\frac{1}{\overline{\nu}}\sum_{k=1}^{\overline{\nu}}\Omega_k''+\cdots,\quad\text{(B14)}$$

$$\Omega_N=-\frac{1}{\overline{\nu}}\left(\Delta\overline{\nu}-\frac{\phi}{2\pi}\right)\Omega'(1)+\cdots.\quad\text{(B15)}$$

Finally, collecting all the terms and having done similar calculations for the case of $\Delta\overline{\nu}<\phi/2\pi<1$, we obtain

$$\omega(\phi,\overline{\nu})=1+\frac{\Omega'(0)-\Omega'(1)}{12\overline{\nu}^2}\left[-1+\frac{3\phi}{\pi}\left(1-\frac{\phi}{2\pi}\right)\right]+\frac{\Omega'(1)}{2\overline{\nu}^2}\times\begin{cases}(1-\Delta\overline{\nu})\left(\dfrac{\phi}{\pi}-\Delta\overline{\nu}\right), & 0<\dfrac{\phi}{2\pi}<\Delta\overline{\nu},\\ \Delta\overline{\nu}\left(1+\Delta\overline{\nu}-\dfrac{\phi}{\pi}\right), & \Delta\overline{\nu}<\dfrac{\phi}{2\pi}<1.\end{cases}\quad\text{(B16)}$$

In the particular case of a symmetric pulse shape with $\Omega'(1)=-\Omega'(0)$ the full amplitude of the ϕ variation of $\omega(\phi,\overline{\nu})$ from Eq. (B16) is given by Eq. (16).

[1] B. Yu. Sharkov, D. G. Koshkarev, M. D. Churazov, N. N. Alexeev, M. M. Basko, A. A. Golubev, and P. R. Zenkevich, Nucl. Instrum. Methods Phys. Res. A **415**, 20 (1998).
[2] N. Angert, Nucl. Instrum. Methods Phys. Res. A **415**, 236 (1998).
[3] B. Yu. Sharkov, N. N. Alekseev, M. D. Churazov, A. A. Golubev, D. G. Koshkarev, and P. R. Zenkevich, Nucl. Instrum. Methods Phys. Res. A **464**, 1 (2001).
[4] See http://www-new.gsi.de/zukunftsprojekt: ''An International Accelerator Facility for Beams of Ions and Antiprotons,'' Conceptual Design Report, GSI (2001).
[5] M. M. Basko, Phys. Plasmas **7**, 4579 (2000).
[6] N. A. Tahir, D. H. H. Hoffmann, A. Kozyreva, A. Shutov, J. A. Maruhn, U. Neuner, A. Tauschwitz, P. Spiller, and R. Bock, Phys. Rev. E **62**, 1224 (2000).
[7] D. G. Koshkarev and M. D. Churazov, At. Energ. **91**, 47 (2001).
[8] M. M. Basko, M. D. Churazov, and A. G. Aksenov, Laser Part. Beams **20**, 411 (2002).

[9] A. R. Piriz, N. A. Tahir, D. H. H. Hoffmann, and M. Temporal, Phys. Rev. E **67**, 017501 (2003).
[10] Ya. B. Zel'dovich and Yu. P. Raizer, *Physics of Shock Waves and High-Temperature Hydrodynamic Phenomena* (Academic, New York, 1967).
[11] See National Technical Information Service Document No. DE92014078 (F. L. Addessio, J. R. Baumgardner, J. K. Dukowicz, N. L. Johnson, B. A. Kashiwa, R. M. Rauenzahn, and C. Zemach, CAVEAT: A Computer Code for Fluid Dynamics Problems With Large Distortion and Internal Slip, LA Rep. 10613-MS, Rev. 1, 1992). Copies may be ordered from the National Technical Information Service, Springfield, VA 22161.